Catalysts for the Oxygen Reduction from Heat-Treated Iron(III) Tetramethoxyphenylporphyrin Chloride: Structure and Stability of Active Sites

Hendrik Schulenburg,*,† Svetoslav Stankov,‡ Volker Schünemann,‡ Jörg Radnik,§ Iris Dorbandt,† Sebastian Fiechter,† Peter Bogdanoff,† and Helmut Tributsch*,†

Hahn-Meitner-Institut Berlin, Abteilung Solarenergie 5, Glienicker Strasse 100, D-14109 Berlin, Germany, Institut für Physik, Medizinische Universität zu Lübeck, Ratzeburger Allee 160, D-23538 Lübeck, Germany, Institut für Angewandte Chemie Berlin-Adlershof, Richard-Willstätter Strasse 12, D-12489 Berlin, Germany

Received: March 19, 2003; In Final Form: June 9, 2003

Structure and stability of an iron-based catalyst for the oxygen reduction reaction, prepared by heat treatment of carbon-supported iron(III) tetramethoxyphenylporphyrin chloride (FeTMPP−Cl), were investigated. The oxygen reduction in acid electrolyte was examined with the rotating (ring) disk electrode. The measurements confirmed that H_2O_2 is generated as a byproduct of the oxygen reduction. The structural elucidation of the catalyst showed that the porphyrin decomposes during heat treatment. Nitrogen atoms of the heat-treated porphyrin become bonded at the edge of graphene layers as pyridine- and pyrrole-type nitrogen. Two Fe^{3+} components as well as metallic, carbidic and oxidic iron were detected by Mössbauer spectroscopy. An electrochemical longevity test and two degradation experiments with sulfuric acid and H_2O_2 showed that H_2O_2 causes the degradation of active sites. A 6-fold coordinated Fe^{3+} compound seems to be responsible for the catalytic activity. Only 8% of the primary iron content is present in the active iron component.

1. Introduction

Carbon-supported, heat-treated iron−N_4 macrocycles[1−6] are active catalysts for the oxygen reduction reaction, which can be formulated as a 4-electron-transfer reaction.

$$O_2 + 4H^+ + 4e^- \rightarrow 2H_2O \qquad (1)$$

These iron-based catalysts are discussed as cathode material for polymer electrolyte membrane fuel cells (PEMFCs) and direct methanol fuel cells (DMFCs). Platinum catalysts, which are commonly used for these applications, are expensive, of limited availability and become depolarized by methanol. The latter is a severe drawback in DMFCs where a fraction of methanol diffuses from the anode across the membrane toward the cathode. At the cathode platinum catalysts oxidize methanol electrochemically. This effect leads to a loss of cell voltage. Iron-based catalysts reduce oxygen selectively in the presence of methanol[2,6] and are also cheaper than platinum.

Among the most active and promising iron-based catalysts are carbon-supported and heat-treated iron(III) tetramethoxyphenylporphyrin chloride (FeTMPP−Cl) catalysts (Figure 1). Catalytic activity and structure of these compounds have been investigated by Gojkovic[1,6] and Lefèvre.[3,4] Gojkovic prepared FeTMPP−Cl catalysts with Black Pearls (Cabot) as carbon support and showed that highest activity is achieved if the supported porphyrin is pyrolyzed at temperatures between 700 and 1000 °C.[1] A rotating ring disk study by the same group[7] showed that in acid media oxygen is reduced to water and hydrogen peroxide. If the catalysts were prepared at a pyrolysis temperature of 1000 °C, iron particles could be detected by cyclic voltammetry and TEM images.[1] Very few iron particles could be detected at lower pyrolysis temperatures.

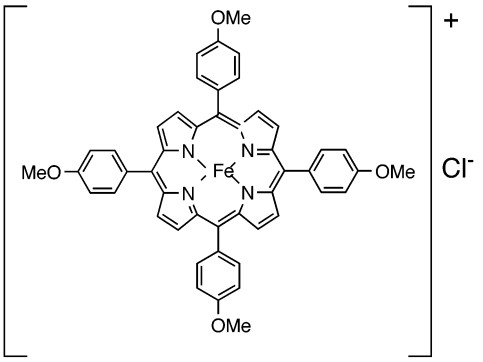

Figure 1. Iron(III) tetramethoxyphenylporphyrin chloride (FeTMPP−Cl).

Lefèvre[3,4] prepared FeTMPP−Cl catalysts by pyrolyzing perylene tetracarboxylic dianhydride together with the porphyrin. The iron content and pyrolysis temperature were varied. Time-of-flight secondary ion mass spectroscopy (Tof-SIMS) showed a correlation between the catalytic activity and the presence of $FeN_xC_y^+$ ions. From these results and XPS measurements of similar catalysts[8] it was concluded that the active sites have a phenantroline-type structure when prepared at temperatures ≥800 °C.[4] According to this model nitrogen is bonded as pyridine-type nitrogen in a graphene layer and is coordinated to iron. Still unknown is the oxidation state and the coordination number of iron in the active site.

A disadvantage of iron-based catalysts is the moderate or even low long-term stability. Various authors have shown that the stability can be improved by choosing appropriate heat treatment

* Corresponding authors. Present address: Max-Planck-Institut für Kohlenforschung, AK Reetz, Kaiser-Wilhelm-Platz 1, 45470 Mülheim an der Ruhr, Germany. Tel. +49-208-306-2393 Fax. +49-208-306-2985 (H.Schulenburg). E-mail addresses: schulenburg@mpi-muelheim.mpg.de (H.Schulenburg), tributsch@hmi.de (H.Tributsch).

† Hahn-Meitner-Institut Berlin.

‡ Medizinische Universität zu Lübeck.

§ Institut für Angewandte Chemie Berlin-Adlershof.

10.1021/jp030349j CCC: $25.00
Published on Web 07/19/2003

conditions.[6,9,10] But up to now no iron-based catalyst is known that is stable enough for practical application in PEMFCs or DMFCs. Little is known about the processes that led to the degradation. Gouérec[11,12] studied the stability of carbon-supported cobalt−N4 macrocyles, heat-treated at 800 °C. It was found that after a longevity test the metal concentration decreased beyond the detection limit of XPS. A protonation of nitrogen atoms and the formation of NO_3^- were proposed.

In this work a carbon-supported and heat-treated FeTMPP−Cl catalyst was investigated.

The aim was an improved understanding of the structure of the catalytic site and the chemical cause for the degradation of active sites.

We will show that probably a 6-fold coordinated Fe^{3+} compound is responsible for the catalytic activity and that hydrogen peroxide, which is a byproduct of the oxygen reduction, causes the degradation of active sites.

2. Experimental Section

Catalyst Preparation. The preparation is similar to the procedure described by Gojkovic.[1] A 50 mg sample of FeTMPP−Cl (Aldrich) was dissolved in 100 mL of acetone and magnetically stirred for 2 h. (Samples that were investigated by means of Mössbauer spectroscopy were prepared with ^{57}Fe-enriched FeTMPP−Cl supplied from Porphyrin Systems. The degree of enrichment was >94% ^{57}Fe.) Black Pearls (Cabot, 100 mg) were added. The suspension was magnetically stirred at room temperature. After 20 h of stirring the suspension was filtered under reduced pressure over a Teflon filter (pore size 0.2 μm). The dry residue was heat-treated for 1 h at 900 °C in an argon atmosphere. After heat treatment the catalyst was allowed to cool in argon. The catalyst obtained by this procedure will be called "untreated catalyst" in the following text.

Electrochemical Characterization. The untreated and treated catalysts were characterized by rotating disk electrode (RDE) and rotating ring−disk electrode measurements (RRDE). All electrochemical measurements were performed at room temperature in a one-compartment cell. Oxygen-saturated 0.5 M sulfuric acid (Merck) was used as an electrolyte. The counter electrode was platinum, whereas mercury/mercury sulfate (+650 mV vs normal hydrogen electrode, NHE) served as reference. Mirror-polished glassy carbon disk electrodes (3 mm diameter) served as a substrate for the iron-based catalysts. The catalysts were attached to the glassy carbon disk in the following way: 1 mg of catalyst per 100 μL of deionized water and 100 μL of an ethanol Nafion solution (0.2% Nafion) were ultrasonically dispersed for 15 min. A 5 μL aliquot of the suspension was dropped onto the glassy carbon electrode, and the suspension was air-dried at room temperature.

Rotating ring−disk experiments were performed with the same working, reference and counter electrode as the rotating disk measurements. The ring electrode was made of platinum. The radius of the disk electrode was 1.5 mm, and the inner and outer radii of the ring electrode were 2.3 and 5.2 mm, respectively. A theoretical collection efficiency of 0.634 was calculated with the formula given by Albery and Hitchman.[13] The collection efficiency was also determined experimentally. For that purpose the catalyst was attached to the disk electrode and the collection efficiency was determined with an $Fe^{2+/3+}$ redox couple.[14] The experimental collection efficiency was 0.63. For the detection of H_2O_2 a ring potential of 1.4 V (NHE) was applied. All polarization curves were performed between 0.8 and 0.0 V (NHE) at a scan rate of 5 mV/s. Rotation rates were 100, 400, 900, 1600, and 2500 min^{-1}.

Degradation Experiments. Three degradation experiments were performed with the aforementioned catalyst. The different treatments should show how fast the activity decreases in a longevity test and if an acid electrolyte or hydrogen peroxide leads to a degradation of activity. The treatment with sulfuric acid should simulate the conditions in PEMFCs or DEMFCs where catalysts are also exposed to a highly acidic electrolyte. The hydrogen peroxide treatment should show if this byproduct of the oxygen reduction causes the degradation of the catalyst.

1. Longevity Tests at 0.7 V (NHE). Two longevity tests were performed. In the first test the untreated catalyst was attached to a glassy carbon electrode (see electrochemical characterization). The electrolyte was oxygen-saturated 0.5 M sulfuric acid (Merck). A constant potential of 0.7 V (NHE) was applied for 100 h, and the current was recorded. During the measurement oxygen was passed over the electrolyte. The second longevity test was performed as half-cell measurement using the same counter and reference electrodes. The gas diffusion electrode was prepared by grinding 150 mg of catalyst and 30 mg of Teflon. The catalyst/Teflon mixture was rolled onto a gas permeable carbon paper. The size of the gas diffusion electrode was 0.71 cm^2. During the longevity test oxygen was led to the electrode at a pressure of 1 bar. A potential of 0.7 V (NHE) was applied for 100 hours and the current was recorded. Both longevity tests were performed at room temperature.

2. Acid Treatment. At room temperature 25 mg of the untreated catalyst were stirred magnetically in 30 mL of sulfuric acid (c = 0.5 mol/L). Small gas bubbles were visible at the beginning of the acid treatment. After 100 h the suspension was filtered and the residue was air-dried at room temperature.

3. Hydrogen Peroxide Treatment. A 20 mg sample of the acid treated catalyst was treated drop by drop with 30 mL of an aqueous H_2O_2 (30%) solution (Merck). The suspension was stirred and cooled in a water bath at room temperature. A vigorous gas evolution was observed, indicating a catalytic decomposition of H_2O_2. After stirring the suspension for 100 h, it was filtered and the residue was air-dried at room temperature.

Thermogravimetry. Thermogravimetry of the unpyrolyzed catalyst was performed with a Netzsch STA 409C thermobalance. The sample was heated in an argon flow (80 mL/min) at a heat rate of 20 K/min.

X-ray Photoelectron Spectroscopy (XPS). XP spectra were recorded with a Fisions ESCALAB220 iXL spectrometer working with a monochromatic Al Kα X-ray source. The samples were fixed with a double sticking C-tape to the sample holder and measured with a 150 μm spot to avoid an influence of the C-tape on the spectra. The spectra were deconvoluted with mixed Gauss−Lorentzian curves.

^{57}Fe-Mössbauer Spectroscopy. Mössbauer spectra were recorded using a conventional spectrometer in the constant acceleration mode. Isomer shifts are given relative to α-Fe at room temperature. The Mössbauer spectra were analyzed by a least-squares fit using Lorentzian shape.

Neutron Activation Analysis (NAA). Measurements were performed at the BER II reactor at the Hahn-Meitner-Institut Berlin. The samples were irradiated for 24 h with a neutron flux density of 6×10^{12}/(s cm^2). The decay time of the activated samples was 3 days. $K_3[Fe(CN)_6]$ was used as reference material.

3. Results

Electrochemical Characterization. The catalytic activity of the untreated and treated catalysts was calculated from RDE

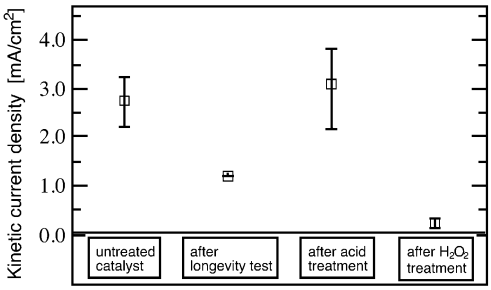

Figure 2. Untreated and treated FeTMPP−Cl catalysts: Kinetic current densities at 0.7 V (NHE) for the oxygen reduction reaction, determined by rotating disk electrode measurements. Electrolyte was oxygen saturated 0.5 M sulfuric acid.

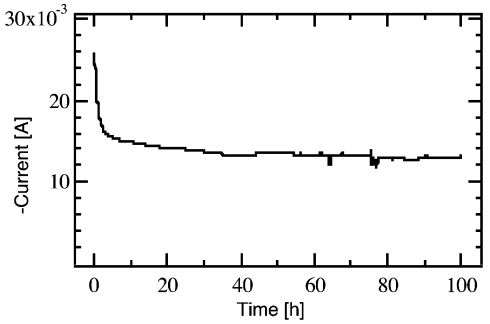

Figure 3. Longevity test at 0.7 V (NHE). Electrolyte was oxygen saturated 0.5 M sulfuric acid. Gas diffusion electrode was prepared from untreated FeTMPP−Cl catalyst.

polarization curves using the Levich−Koutecky equation

$$1/i = 1/i_{kin} + 1/i_d = 1/i_{kin} + 1/B\omega^{1/2} \qquad (2)$$

assuming a first-order kinetic with respect to oxygen. In eq 2 i is the current density, i_{kin} is the kinetic current density, i_d is the diffusion-limited current density, and ω is the rotation rate. The kinetic current density is proportional to the activity of the catalysts. The constant B is $0.62nFcD^{2/3}\nu^{-1/6}$, where c is the bulk concentration of oxygen ($c = 1.1\times 10^{-6}$ mol cm^{-3}), D is the diffusion constant of oxygen ($D = 1.8 \times 10^{-5}$ cm^2 s^{-1}), and ν is the kinematic viscosity of the electrolyte ($\nu = 10^{-1}$ cm^{-2} s^{-1}). Tafel graphs were obtained by plotting log(i_{kin}) versus potential. Kinetic current densities were compared at 0.7 V (NHE) where the oxygen reduction is mainly under kinetic control. This cathode potential seems to be appropriate for PEMFCs with FeTMPP−Cl catalysts. At 0.7 V (NHE) a kinetic current density of 2.7 mA/cm^2 for the untreated catalyst is obtained (Figure 2). After the 100 h longevity test at 0.7 V (NHE) a kinetic current density of 1.2 mA/cm^2 is observed. A similar decrease in the current density was also observed in the half-cell longevity test (Figure 3). The acid treatment had no negative effect, whereas the H_2O_2 treatment led to a sharp decrease in activity. A Tafel slope of 61 ± 4 mV/dec was measured for all catalysts, suggesting that the rate determining step of the reduction is the same.

The selectivity of the oxygen reduction was analyzed with the ring disk technique. All catalysts show a ring current in the potential range of 0.8−0 V (NHE). The amount of generated hydrogen peroxide was calculated by eq 3,[15] where I_r is the

$$\%\ H_2O_2 = 200\ (I_r/N)/((I_r/N) + |I_d|) \qquad (3)$$

ring current, I_d is the disk current, and N is the collection efficiency of the RRDE. Equation 3 was derived for a parallel mechanism in which oxygen is reduced to water and hydrogen peroxide. Iron-based catalysts follow a more complex mechanism in which H_2O_2 is also reduced electrocatalytically and is decomposed catalytically.[7,16] In that case the real hydrogen peroxide generation is higher than calculated by eq 3.[16] Nevertheless, a qualitative comparison of the values is possible. Within the error limit all catalysts produce the same amount of hydrogen peroxide, according to eq 3 about 10−11% at 0.7 V (NHE).

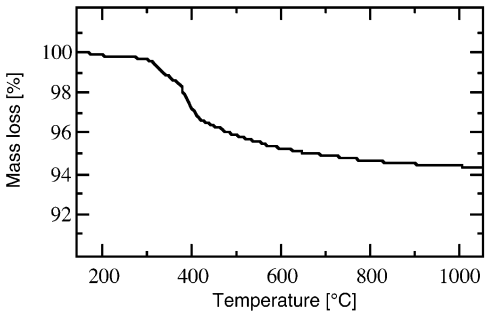

Figure 4. Thermogravimetry under argon flow of the untreated FeTMPP−Cl catalyst before heat treatment. Heat rate 20 K/min.

TABLE 1: Neutron Activation Analysis: Fe Content of the Untreated and Treated FeTMPP−Cl Catalysts

catalyst	Fe content
untreated	2.05 ± 0.12%
after acid treatment	0.47 ± 0.05%
after acid and H_2O_2 treatment	0.52 ± 0.05%
after longevity test	0.39 ± 0.08%[a]

[a] Value was calculated for the pure catalyst without Teflon from the gas diffusion electrode.

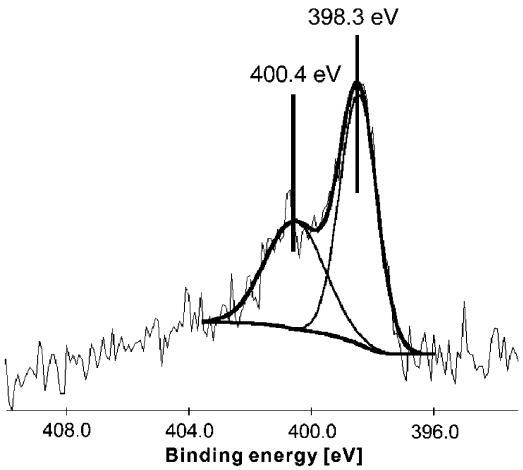

Figure 5. Nitrogen 1s spectrum of the untreated FeTMPP−Cl catalyst.

Thermogravimetry. By means of thermogravimetry it is possible to observe the mass loss of the supported porphyrin during the heat treatment. Figure 4 shows that the decomposition of the porphyrin already starts at 300 °C. The largest mass change is observed between 300 and 400 °C. At the pyrolysis temperature of 900 °C the total mass loss is 6%. The result indicates that at least a fraction of the porphyrin decomposes during the heat treatment and forms new compounds.

Neutron Activation Analysis (NAA). The results of the NAA are summarized in Table 1. The untreated catalyst has an iron content of 2.05 ± 0.12%. After leaching with sulfuric acid the iron content is lowered to 0.47 ± 0.05%. The further treatment of the acid-leached catalyst with hydrogen peroxide does not change the iron content significantly 0.52 ± 0.05%. The iron content in the catalyst after the longevity test is similar 0.39 ± 0.08%.

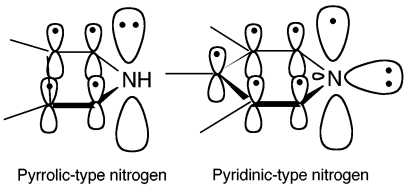

Figure 6. Pyrrole- and pyridine-type nitrogen.

TABLE 2: X-ray Photoelectron Spectroscopy: N1s Binding Energies of the Catalysts

catalyst	peak 1	peak 2
untreated	398.3 eV	400.4 eV
after acid treatment	398.3 eV	400.8 eV
after H_2O_2 treatment	398.5 eV	400.1 eV
after longevity test	398.5 eV	400.8 eV

X-ray Photoelectron Spectroscopy (XPS). The N1s spectra of all samples can be deconvoluted with two peaks. As an example, Figure 5 shows the deconvoluted spectrum of the untreated catalyst. Peak 1 (Figure 6 and Table 2) with a binding energy of 398.3 eV can be assigned to pyridine-type nitrogen. Peak 2 with a binding of 400.4 eV is characteristic for pyrrole-type nitrogen.[17] The nitrogen atoms are bonded at the edge of graphene layers forming covalent bonds with two carbon atoms. Generally, these types of nitrogen were found after the carbonization of nitrogen-containing organics.[18,19] They were also found in other iron-based catalysts.[8,20,21]

^{57}Fe-Mössbauer Spectroscopy. *Untreated Catalyst (Figure 7).* The spectrum of the untreated catalyst can be deconvoluted with three subspectra. Component *C*, the sextet, has a value of 20.7 T for the hyperfine field, which is also observed for θ-Fe_3C.[22] The singlet *M* with an isomer shift of 0.0 mm/s at 4.2 K (Table 3) can be assigned to superparamagnetic metallic iron particles. Because no metal particles could be observed by TEM, the particles seem to be smaller than 1.5 nm (TEM images not shown). The third component Ox is a doublet with an isomer shift of 0.34 mm/s and a quadrupole splitting of 1.01 mm/s. This component may be assigned to α-Fe_2O_3. Measurements of various iron oxides from Kündig[23] show that the isomer shift and quadrupole splitting of α-Fe_2O_3 strongly depend on the particle size. For a particle size of less than 10 nm an isomer shift of 0.34 mm/s and a quadrupole splitting of 0.98 mm/s were found. These values are in agreement with subspectrum Ox.

Catalyst after Acid Treatment (Figure 8). After acid treatment the activity of the catalyst did not decrease. The lines assigned to superparamagnetic metallic iron and θ-Fe_3C have disappeared. The acid leached both components out. Iron oxides, like α-Fe_2O_3 are poorly soluble in acids, therefore the oxide can still be observed in the spectrum. A good fit of the spectrum is possible with two other subspectra, called A and B, which show isomer shifts of 0.46 and 0.12 mm/s. Both can be assigned to high spin Fe $^{3+}$ components. According to the isomer shifts A is probably 4-fold and B 6-fold coordinated. Components A and B show very large quadrupole splittings (2.75 and 2.93 mm/s), which point to a large electric field gradient at the iron nucleus. Surface atoms are likely to show a large quadrupole splitting, due to the highly asymmetric environment. A and B cannot be assigned to iron oxides because the quadrupole splittings are

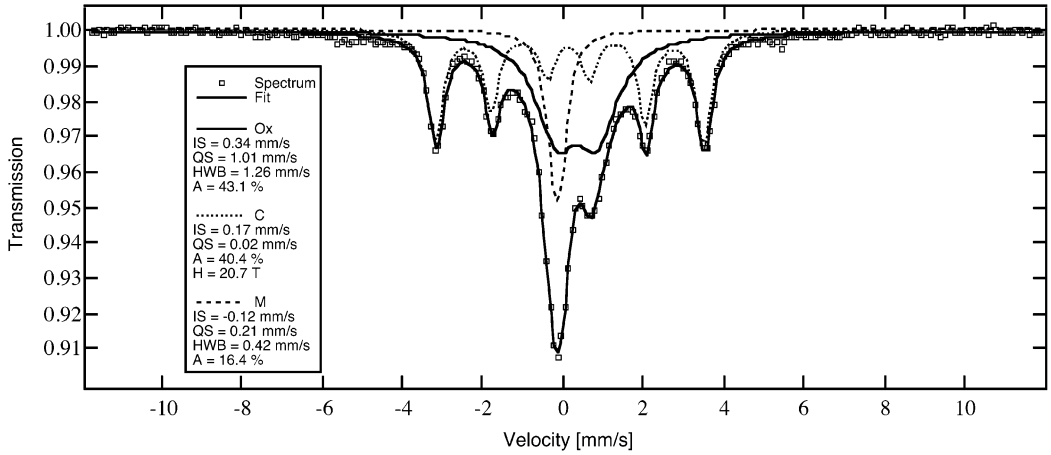

Figure 7. Room temperature ^{57}Fe-Mössbauer spectrum of the untreated FeTMPP−Cl catalyst.

TABLE 3: Mössbauer Parameter of the Untreated and Treated FeTMPP−Cl CatalystMeasured at 300 K

catalyst	component	isomer shift (mm/s)	quadrupole splitting (mm/s)	half-width (mm/s)	rel area (%)
untreated	Ox	0.34	1.01	1.26	43.1
	C	0.17	0.02		40.4
	M	−0.12	0.21	0.42	16.4
after acid treatment	Ox	0.35	1.14	0.71	50.6 (19.7 at 4.2 K)
	A	0.12	2.93	0.58	18.7 (47.0 at 4.2 K)
	B	0.46	2.75	0.76	30.6 (33.3 at 4.2 K)
after H_2O_2 treatment	Ox	0.37	1.02	0.72	55.1
	B	0.34	2.88	0.96	39.3
	I1	0.48	2.13	0.39	5.6
after longevity test	Ox	0.30	1.10	0.85	50.1
	B	0.28	2.92	0.99	41.4
	I2	0.83	1.77	0.41	5.2
	C	0.46	−0.49		3.4

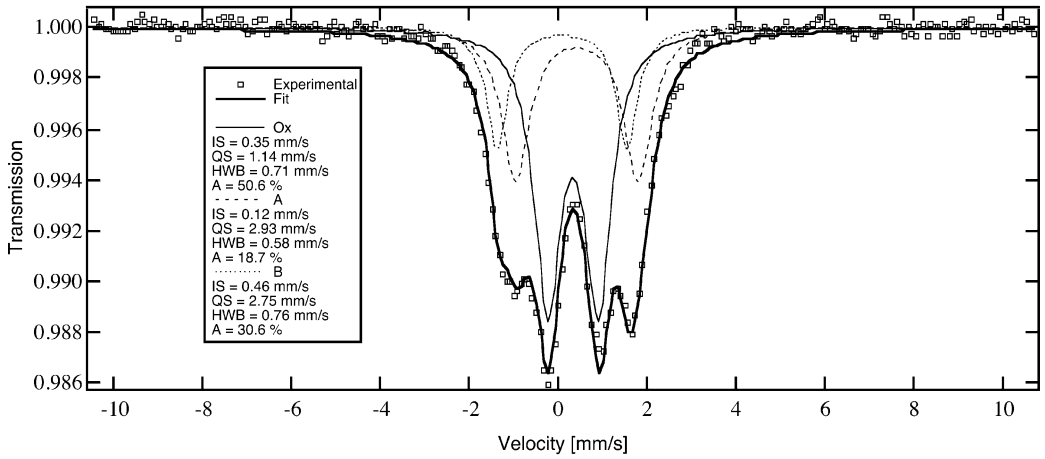

Figure 8. Room temperature ^{57}Fe-Mössbauer spectrum of the acid treated FeTMPP−Cl catalyst.

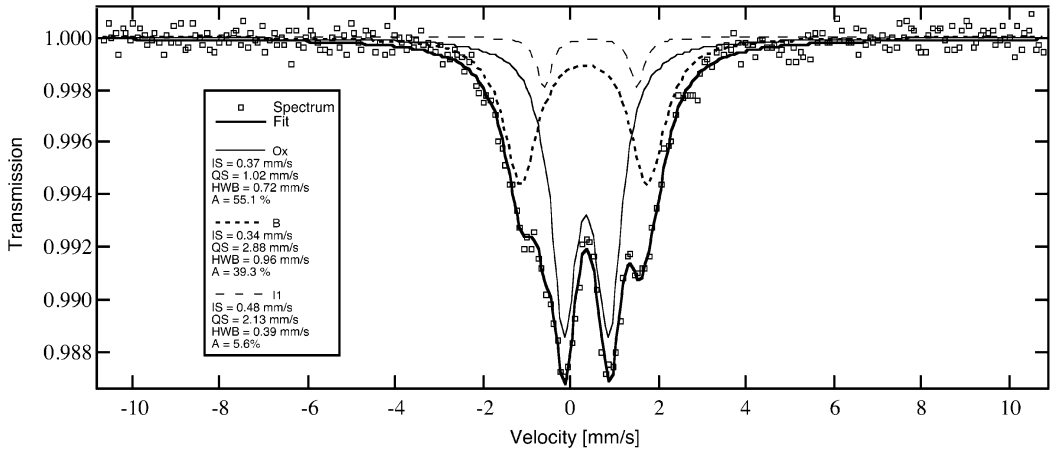

Figure 9. Room temperature ^{57}Fe-Mössbauer spectrum of the H_2O_2 treated FeTMPP−Cl catalyst.

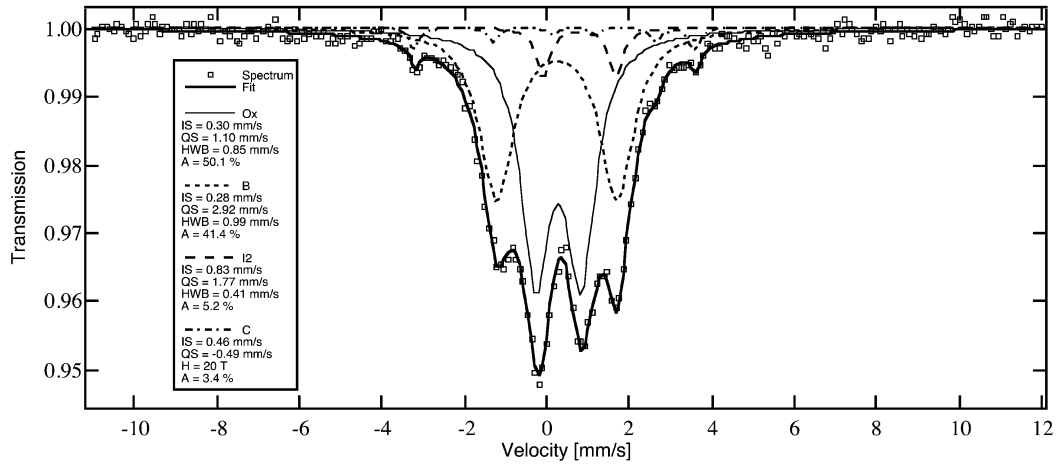

Figure 10. Room temperature ^{57}Fe-Mössbauer spectrum of the FeTMPP−Cl catalyst after longevity test.

much higher than observed for iron oxides, even if the particle size of the oxides is in the nanometer range.[23]

Catalyst after Hydrogen Peroxide Treatment (Figure 9). Exposure of the catalyst to H_2O_2 led to an almost complete loss of activity. The iron oxide (component Ox) and Fe^{3+} component B are still present after the treatment. Component A is no longer observed. The isomer shift of component B (0.34 mm/s) has changed significantly compared to the sample that was just treated with acid (0.46 mm/s). That can be explained by a chemical reaction of the ligands or different metal to ligand bond lengths. The half-width of component B is also considerably higher, indicating that the structure has become less ordered. A small quantity of the new compound I1 appears, which may be assigned to an impurity or reaction product due to the hydrogen peroxide treatment.

Catalyst after Longevity Test (Figure 10). After the half-cell longevity test the catalytic activity is about 50% lower than the activity of the untreated catalyst. The spectrum is similar to the spectrum after the acid and hydrogen peroxide treatment (Figure 9). The dominant subspectra in both cases can be assigned to an iron oxide (component Ox) and component B. Component A is not observed. The isomer shift and half-width of component

TABLE 4: Mössbauer Spectroscopy: Iron Components in the Catalysts

catalyst	iron oxides	iron carbides	metallic iron	Fe^{3+} components
untreated	α-Fe_2O_3	θ-Fe_3C	Fe	
after acid treatment	α-Fe_2O_3			coord nos. 6 and 4
after H_2O_2 treatment	α-Fe_2O_3			coord no. 6
after longevity test	α-Fe_2O_3	θ-Fe_3C		coord no. 6

B have changed compared to the sample which was treated with acid (Figure 8). The change of these parameters indicates that reactions in the coordination sphere of Fe^{3+} occur and that the structure has become less ordered. This was also found after the hydrogen peroxide treatment. Small amounts of carbidic iron (component C) are also present in this sample, as well as the impurity compound I2.

4. Discussion

Stability of the Active Sites. The electrochemical characterization of the catalysts showed that all samples have a Tafel slope of about 61 mV/dec and generate similar amounts of hydrogen peroxide. Therefore, it is likely that the active site of all catalysts is the same or at least similar. The degradation tests showed clearly that acid (without an applied potential) has no negative effect on the activity. The active sites, however, degrade if they are exposed to hydrogen peroxide. That is the case after the hydrogen peroxide treatment and during the longevity test with an applied potential. The degradation after the hydrogen peroxide treatment was more distinct than the degradation after the longevity tests. That can be explained by the higher concentration of H_2O_2 (30%) to which the catalyst was exposed at the hydrogen peroxide treatment. During the longevity tests, where H_2O_2 is only generated as a byproduct of the oxygen reduction, the concentration is expected to be much lower.

Active Component. The results of the structural elucidation by Mössbauer spectroscopy are summarized in Table 4. Metallic iron, θ-Fe_3C and α-Fe_2O_3 were found in the untreated sample. Metallic iron and Fe_3C are inactive and not stable in acid media. Some iron oxides[24,25] and especially mixed oxides[26,27] show activity for the oxygen reduction in alkaline media. Recently Jaouen[28] found evidence for a low activity of iron oxides/hydroxides even in acid media. However, activity of α-Fe_2O_3 was never reported; therefore, we regard it as inactive. The activity obviously originates from one or both of the remaining Fe^{3+} components. These components were not considered in the deconvolution of the untreated catalyst. Anyway it is likely that they are masked by the lines of metallic iron and θ-Fe_3C if their relative contribution is below 5% in the 300 K spectra. There is no other way to explain the activity of the untreated sample without Fe^{3+} component A or B. Whether component A, B, or both are connected with the activity will now be discussed.

Hypothesis 1: Fe^{3+} Component A Active. If we assume that component A is active, the electrochemical and spectroscopic results can be interpreted as follows. Component A is present in the untreated sample and is responsible for the activity. After the acid treatment the metallic and carbidic iron is leached out and component A can be detected spectroscopically. After undergoing hydrogen peroxide treatment the active compound is destroyed and therefore the activity declines. The following problems arise with that hypothesis. After the hydrogen peroxide treatment the catalyst shows a much lower activity, but is still active although component A has disappeared completely. Consequently, there must be another compound that causes the activity of the catalyst after the hydrogen peroxide treatment.

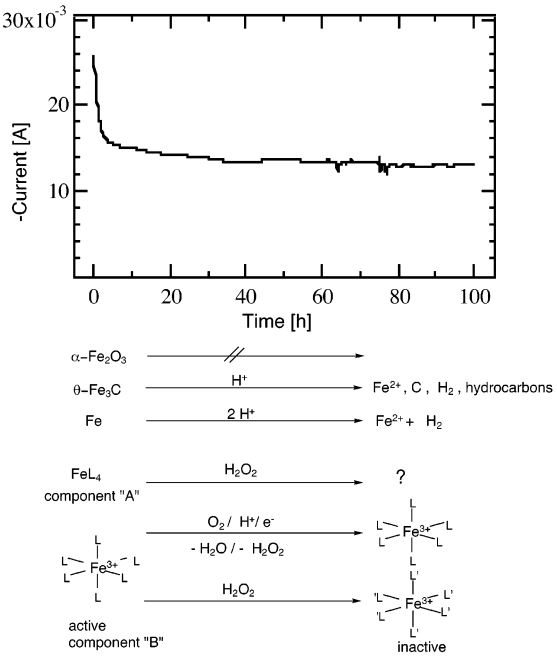

Figure 11. Longevity test of the untreated FeTMPP−Cl catalyst at 0.7 V (NHE) (above). Proposed model for the degradation of the active iron component and reactions of inactive iron components during the longevity test.

A similar problem arises interpreting the spectrum after the longevity test. It is plausible that component *A* is destroyed during the test because hydrogen peroxide is a byproduct of the oxygen reduction. But it remains unclear why component A disappeared completely and the activity of the catalyst is only lowered by 50%.

Hypothesis 2: Fe^{3+} Component B Active. If we thus assume that component A is inactive, oxygen reduction is caused by the remaining component B. After the hydrogen peroxide treatment and the longevity test the activity decreases. In both cases this can be explained by degradation of component B through hydrogen peroxide. The degradation may be due to a chemical modification of the ligands of that component. According to this hypothesis the degradation of the catalyst during the longevity test is summarized in Figure 11. At the beginning metallic iron, iron oxides and carbides, as well as the components A and B are present. The poor soluble α-Fe_2O_3 does not react, whereas metallic iron particles and carbides were dissolved by acid corrosion. The active component B reduces oxygen to water and hydrogen peroxide. A part of the active sites is destroyed by hydrogen peroxide. The inactive component A is completely destroyed by the hydrogen peroxide generated. The product of degradation is unknown. The hypothesis that component B is catalyticly active seems to allow the interpretation of the electrochemical and spectroscopic results without contradictions.

Hypothesis 3: Fe^{3+}Components A and B Active. After a SIMS study of iron-based catalysts by Lefèvre[3] it was proposed that two different active sites exist simultaneously. These were labeled FeN2/C and FeN4/C sites. Are these identical with components A and B that were found in this work? Different active sites usually show different kinetics; thus A and B should lead to different Tafel slopes and H_2O_2 generations. In the untreated and acid-treated samples both components A and B are present. A Tafel slope of 60 mV/dec and a H_2O_2 generation of 10% were found. Similar values were also observed for the degraded samples where only component B is present. Therefore it seems that only compound B is active. On the other hand, it

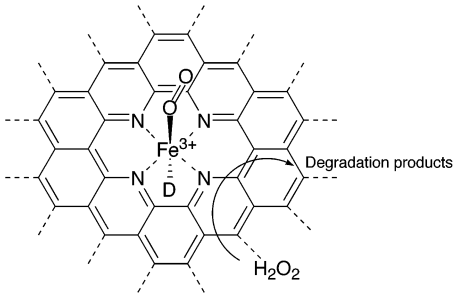

Figure 12. Proposed model for the structure of the active site. Hydrogen peroxide may destroy the active sites by oxidation of nitrogen ligands.

is possible that component A is much less active than B. In that case the kinetics would always be dominated by B. It is also thinkable that the oxygen reduction kinetics of A and B is very similar by chance. Thus the existence of two active sites is also possible, but an activity of component *A* cannot be proofed in this work.

Structure of Active Component. The nature of the active component B cannot be determined completely by Mössbauer spectroscopy and XPS; therefore the following proposal for the structure still remains speculative. The isomer shift that is observed in the Mössbauer spectra is typical for iron in the oxidation state +3 probably 6-fold coordinated. The quadrupole splitting of the active component B is too high for iron oxides, so the formation of Fe^{3+} coordinated to nitrogen may be proposed. From Tof-SIMS measurements of pyrolyzed Fe-TMPP−Cl catalysts Lefèvre[3,4] also proposed that FeC_xN_y is responsible for the activity. EXAFS measurements on similar catalysts by Bron[29] and Bouwkamp-Wijnoltz[30] also suggest that FeN_x sites are responsible for the catalytic activity. A coordination of iron with 3 or 4 nitrogen atoms was calculated from these measurements.[29,30] The Mössbauer measurements in this work suggest that iron is 6-fold coordinated in the active compound. For geometrical reasons it is very unlikely that more than four nitrogen atoms are coordinated to an iron center, because the nitrogen ligands are bonded in graphene layers. The missing ligands could be adsorbed oxygen or an interaction with an adjacent graphene layer (Figure 12). It should also be mentioned that the treated catalysts were exposed to in situ conditions or at least conditions that are similar to in situ. Mössbauer spectroscopy and XPS of the catalyst were performed under ex situ conditions. Thus the in situ structure of the active site is expected to be different.[30] In particular, the oxidation state of iron may be different, because a multielectron reduction from an Fe^{3+} site seems unlikely. Further in situ Mössbauer and EXAFS measurements are necessary to get more information about the structure under working conditions of the catalysts.

Formation of Active Sites. From Mössbauer and XPS data of the untreated and treated catalyst one gets the following image of the pyrolysis process. Before heat treatment, FeTMPP−Cl molecules form one or more layers onto the carbon support. During pyrolysis FeTMPP−Cl throws off hydrogen. C−C and C−N bonds of the macrocycles are breaking. The resulting radicals are more or less mobile and are forming graphene layers, which are not well-defined. Nitrogen atoms of the porphyrin become bonded at the edge of these layers. A small fraction of Fe atoms stays in contact with N atoms and forms active sites. An iron atom of an active site may be integrated in a single disordered graphene layer. However, most Fe atoms of the porphyrin diffuse onto and into the carbon support during the heat treatment. Along the way they collide and metallic Fe as well as Fe_3C particles are formed. Those are usually very small and difficult to detect by TEM. Some iron components oxidize to α-Fe_2O_3 if exposed to air after heat treatment.

Degradation of Active Sites. The NAA results show that hydrogen peroxide does not lead to a leaching of component B after acid treatment because the iron content remains constant. Therefore, a loss of iron is not the reason for the lowered activity. A possible degradation process may be the oxidation of nitrogen atoms by H_2O_2 (Figure 12). Such an oxidation could explain the change of the isomer shifts and the increased half-width that were observed in Mössbauer spectra of the degraded samples. One the other hand, the N1s binding energies of the FeTMPP−Cl catalysts (Table 2) do not change significantly. An oxidation of the nitrogen ligands should influence the N 1s binding energies. An explanation for the unchanged N1s binding energies could be the dissolution of oxidized nitrogen atoms into the electrolyte. A sensitive elemental analysis of the nitrogen content of the catalyst and of the electrolyte after the longevity test could prove this hypothesis.

Yield for Formation of Active Sites. If component B is responsible for the activity, one can estimate the yield for the formation of this component. After the heat treatment the iron content of the catalyst was 2.05%. After exposure to acid, the activity remains constant; thus the content of the active iron component remains constant. Due to leaching of metallic iron and iron carbides the overall iron content is lowered to 0.47%. The inactive components Ox and A are present in the acid-treated sample, too. From the relative areas of the 4.2 K Mössbauer subspectra (Table 3) one can estimate the fraction in which iron is present in the active component B. According to this spectrum, 33% of the iron is bonded in component B. The amount of iron in the active component is then $0.47\% \times 0.33 = 0.16\%$. This shows that even in this synthesis, which is among the best for iron-based catalysts, the yield for the active component is still very low: only 8 iron atoms out of 100 FeTMPP−Cl molecules form the active iron component. A loading of 0.16% is very low compared to metal loadings of carbon supported platinum catalysts for PEMFCs. From RDE measurements[16] it is known that the catalytic activity of heat-treated FeTMPP−Cl catalysts is about 1 order of magnitude lower than of commercial platinum catalysts (20%Pt/C from E-TEK Inc.). Therefore the catalytic activity per metal atom seems to be considerably higher for heat-treated FeTMPP−Cl. More efficient preparation routes of the active iron component may lead to catalysts that are more active than supported platinum catalysts.

5. Conclusions

From the electrochemical characterization and structural elucidation of carbon-supported and heat-treated FeTMPP−Cl catalysts the following conclusions can be drawn.

- Superparamagnetic metallic iron, θ-Fe_3C, α-Fe_2O_3 and two unknown Fe^{3+} compounds are present in the catalyst.
- Nitrogen is bonded at the edge of graphene layers as pyrrole- and pyridine-type nitrogen.
- A 6-fold coordinated Fe^{3+} compound is probably responsible for the catalytic activity.
- About 8% of the nominal Fe content forms the active iron component.
- Hydrogen peroxide causes the degradation of FeTMPP−Cl catalysts.
- The decrease of catalytic activity during longevity tests can also be explained with a degradation by H_2O_2, which is a byproduct of the oxygen reduction.

Acknowledgment. We thank D. Alber for NAA measurements and the BMBF (contract no. 0327067B) and Daimler-Chrysler AG for financial support.

References and Notes

(1) Gojkovic, S. Lj.; Gupta, S.; Savinell, R. F. *J. Electrochem. Soc.* **1998**, *145*, 3493.

(2) Gupta, S.; Tryk, D.; Zecevic, S. K.; Aldred, W.; Guo, D.; Savinell, R. F. *J. Appl. Electrochem.* **1998**, *28*, 673.

(3) Lefèvre, M.; Dodelet, J. P.; Bertrand, P. *J. Phys. Chem. B* **2002**, *106*, 8705.

(4) Lefèvre, M.; Dodelet, J. P.; Bertrand, P. *J. Phys. Chem. B* **2000**, *104*, 11238.

(5) Bouwkamp-Wijnoltz, A. L.; Visscher, W.; van Veen, J. A. R. *Electrochim. Acta* **1998**, *43*, 3141.

(6) Gojkovic, S. Lj.; Gupta, S.; Savinell, R. F. *J. Electranal. Chem.* **1999**, *462*, 63.

(7) Gojkovic, S. Lj.; Gupta, S.; Savinell, R. F. *Electrochim. Acta* **1999**, *45*, 889.

(8) Faubert, G.; Côté, R.; Dodelet, J. P.; Lefèvre, M.; Bertrand, P. *Electrochim. Acta* **1999**, *44*, 2589.

(9) Faubert, G.; Lalande, G.; Côté, R.; Guay, D.; Dodelet, J. P.; Weng, L. T.; Bertrand, P.; Dénès, G. *Electrochim. Acta* **1996**, *41*, 1689.

(10) Lalande, G.; Faubert, G.; Côté, R.; Guay, D.; Dodelet, J. P.; Weng, L. T.; Bertrand, P. *J. Power Sources* **1996**, *41*, 1689.

(11) Gouérec, P.; Savy, M. *Electrochim. Acta* **1999**, *44*, 2653.

(12) Gouérec, P.; Biloul, A.; Contamin, O.; Scarbeck, G.; Savy, M.; Riga, J.; Weng, L. T.; Bertrand, P. *J. Electroanal. Chem.* **1997**, *422*, 61.

(13) Albery, W. J.; Hitchman, M. L. *Ring-disc Electrodes*; Clarendon Press: Oxford, U.K., 1971; p 22.

(14) Alonso-Vante, N.; Tributsch, H.; Solorza-Feria, O. *Electrochim. Acta* **1995**, *40*, 567.

(15) Paulus U. A.; Schmidt T. J.; Gasteiger H. A.; Behm, R. J. *J. Electroanal. Chem.* **2001**, *495*, 134.

(16) Schulenburg, H. Ph.D. Thesis, FU Berlin, 2002.

(17) Casanovas J.; Ricart, J. M.; Rubio, J.; Illas F.; Jiménez-Mateos, J. M. *J. Am. Chem. Soc.* **1996**, *118*, 8071.

(18) Pels, J. R.; Kapteijn, F.; Moulijin, J. A.; Zhu, Q.; Thomas, K. M. *Carbon* **1995**, *33*, 1641.

(19) Schmiers, H.; Friebel, J.; Streubel, P.; Hesse, R.; Köpsel R. *Carbon* **1999**, *37*, 1965.

(20) Côte, R.; Lalande, G.; Guay, D.; Dodelet, J. P. *J. Electrochem. Soc.* **1998**, *145*, 2411.

(21) Faubert, G.; Côte, R.; Guay, D., Dodelet, J. P. *Electrochim. Acta* **1998**, *43*, 1969.

(22) Schünemann, V. Ph.D. Thesis, MU Lübeck, 1993.

(23) Kündig, W.; Bömmel, H. *Phys. Rev.* **1966**, *142*, 327.

(24) Vago, E. R.; Calvo, E. J.; Stratmann, M. *Electrochim. Acta* **1994**, *39*, 1655.

(25) Castro, P. A.; Vago, E. R.; Calvo, E. J. *J. Chem. Soc.* **1996**, *92*, 3371.

(26) Miura, N.; Hayashi M.; Hyodo, T.; Yamazoe, N. *Mater. Sci. Forum* **1999**, *315*−*3*, 562.

(27) Shimizu, Y.; Matsuda, A.; Miura, N.: Yamazoe, N. *Chem. Lett.* **1992**, 1033.

(28) Jaouen, F.; Marcotte, S.; Dodelet, J. P. *J. Phys. Chem. B* **2003**, *107*, 1376.

(29) Bron, M.; Radnik, J.; Fieber-Erdmann, M.; Bogdanoff, B.; Fiechter, S. *J. Electroanal. Chem.* **2002**, *535*, 113.

(30) Bouwkamp-Wijnoltz, A. L.; Visscher, W.; van Veen, J. A. R.; Boellhaard, E.; van der Kran, A. M.; Tang, S. C. *J. Phys. Chem. B* **2002**, *106*, 12993.